



Cite this: *J. Mater. Chem. A*, 2023, 11, 691

# A 2D layered cobalt-based metal–organic framework for photoreduction of CO<sub>2</sub> to syngas with a controllable wide ratio range†

Mei-Juan Wei,<sup>†a</sup> Xian-Yan Xu,<sup>†\*b</sup> Jia-Qi Song,<sup>†a</sup> Mei Pan <sup>\*a</sup> and Cheng-Yong Su <sup>\*a</sup>

Photocatalytic CO<sub>2</sub> reduction to syngas (a mixture of CO and H<sub>2</sub>) with adjustable composition is a prospective way to mitigate the energy shortage and the greenhouse effect. Herein, we synthesize a thermally stable two-dimensional cobalt-based metal–organic framework (denoted as “Co-TBAPy”) consisting of cobalt metal centers and H<sub>4</sub>TBAPy (1,3,6,8-tetrakis(*p*-benzoic acid) pyrene) as an organic linker, which exhibits superior CO<sub>2</sub> adsorption capability and a considerable specific surface area. In accordance with the energy levels of [Ru(bpy)<sub>3</sub>]Cl<sub>2</sub>·6H<sub>2</sub>O as a sensitizer, Co-TBAPy is active for photocatalytic reduction of CO<sub>2</sub> to syngas with a wide controllable ratio range between 0.14 and 1.65 under visible-light irradiation. Moreover, the proportion of CO:H<sub>2</sub> = 1:2 and 1:3 favorable for the synthesis of methanol and methane, respectively, can be precisely regulated, which few MOF-based photocatalysts have achieved so far. Furthermore, combined with DFT calculation, we reveal the influence of the water content of the reaction system in the process of photocatalytic CO<sub>2</sub> reduction to produce a controllable proportion of syngas, which is often a profound while elusive factor in photoreduction reactions. This work provides a feasible concept for the design and application of Co-MOF materials for the photoreduction of CO<sub>2</sub> to syngas in practical industrial fields.

Received 16th October 2022  
Accepted 29th November 2022

DOI: 10.1039/d2ta08092c

rsc.li/materials-a

## Introduction

Nowadays, the storage and transformation of carbon dioxide (CO<sub>2</sub>) are two promising approaches to reduce the excessive emission of CO<sub>2</sub> and ease immoderate consumption of fossil resources.<sup>1</sup> Converting CO<sub>2</sub> into value-added chemicals or fuels by artificial photosynthesis is recognized as a reliable way to utilize CO<sub>2</sub> and store solar energy simultaneously. Since CO<sub>2</sub> reduction involves multi-electron processes and competition of hydrogen evolution, the photoreduction products of CO<sub>2</sub> are diverse, including CH<sub>4</sub>, CH<sub>3</sub>OH, HCOOH, CO, H<sub>2</sub>, *etc.*<sup>2,3</sup> To our knowledge, syngas, a mixture of CO and H<sub>2</sub>, is a significant feedstock for the synthesis of high-value added fuels and chemicals by Fischer–Tropsch processes. For actual industrial applications, definite ratios of syngas correspond to certain products. Typically, syngas with the ratio of CO:H<sub>2</sub> = 1:1, 1:2 and 1:3 can be utilized to synthesize alcohol, methanol and

methane, respectively.<sup>4</sup> However, the traditional preparation of syngas through a water gas shift reaction requires harsh conditions and might result in syngas with unsuitable ratios, which restrict its practical industrial application.<sup>5–9</sup>

Therefore, the exploration of appropriate catalysts to prepare a tunable composition of syngas under mild conditions is highly attractive. To date, various photocatalysts have been verified to be suitable catalysts for photocatalytic reduction of CO<sub>2</sub> to syngas. For instance, Co-ZIF-9 or Co<sub>3</sub>O<sub>4</sub> can serve as a photocatalyst to photoreduce CO<sub>2</sub> to syngas under visible light with unadjusted ratios.<sup>10</sup> TiO<sub>2</sub> mesoporous hollow spheres decorated with CuPt alloys and MnO<sub>x</sub> and a heterostructured CoAl-layered double hydroxide/MoS<sub>2</sub> nanocomposite photocatalyst (CoAl-LDH/MoS<sub>2</sub>) exhibit excellent performance in CO<sub>2</sub> photoreduction to CO and H<sub>2</sub> with a tunable ratio.<sup>8,11</sup> However, in order to achieve the desired CO:H<sub>2</sub> ratio of syngas, the structure of the above composite photocatalysts must be well modified accordingly, which is complicated and the mechanism behind is difficult to reveal. Consequently, the preparation of visible light driven catalysts that can produce an adjustable ratio of syngas efficiently and the clear clarification of the structure–performance mechanism are still daunting challenges.

Metal–organic frameworks (MOFs), a type of crystalline material composed of metal nodes and organic ligands as linkers, have been widely researched in various fields,<sup>12</sup> such as

<sup>a</sup>MOE Laboratory of Bioinorganic and Synthetic Chemistry, Lehn Institute of Functional Materials, School of Chemistry, Sun Yat-Sen University, Guangzhou 510006, China. E-mail: panm@mail.sysu.edu.cn; cesscy@mail.sysu.edu.cn

<sup>b</sup>College of Chemistry and Civil Engineering, Shaoguan University, Shaoguan 512005, China. E-mail: sofiaaxy@sgu.edu.cn

† Electronic supplementary information (ESI) available. See DOI: <https://doi.org/10.1039/d2ta08092c>

‡ These authors contributed equally to this work and should be regarded as co-first authors.

gas adsorption,<sup>13</sup> luminescence,<sup>14</sup> catalysis,<sup>15–17</sup> *etc.* Thanks to their adjustable cavities, large specific surface area, easy modification of the structure and excellent adsorption performance of CO<sub>2</sub>, some MOFs, like boron imidazolate frameworks (BIF-101) (ref. 18) and (Co/Ru)<sub>n</sub>-UiO67(bpydc),<sup>19</sup> have been reported as excellent heterogeneous photocatalysts for CO<sub>2</sub> photoreduction to syngas. 2D layer-like MOFs due to their readily accessible active sites and facility for mass diffusion exhibit dramatically boosted photocatalysis.<sup>20–24</sup> However, most of the MOF-based photocatalysts are unstable and prone to structural collapse leading to deactivation, and the research on MOF-based catalysts towards CO<sub>2</sub> photoreduction to syngas with tunable ratios is still in infancy.

Transition metals, especially Cu, Co, Zn and Ni with multiple redox states, can provide favorable CO<sub>2</sub> adsorption sites and advantageous catalytic sites.<sup>16,25</sup> Among them, cobalt (Co)-based complexes are not only low-cost,<sup>26</sup> but also applicable as co-catalysts to enhance CO<sub>2</sub> photoreduction by promoting the photogenerated electron separation.<sup>27,28</sup> Moreover, compared with Cu and Ni, Co possesses good binding capacity for both CO<sub>2</sub> and protons, which can serve as promising catalytic sites for CO<sub>2</sub> reduction to syngas. In an attempt to build an efficient CO<sub>2</sub> photoreduction system, an effective electron-transport chain and strong light-harvesting capability are crucial. Generally, pyrene and its derivatives possess rigid extended  $\pi$ -systems, which might display  $\pi$ -conjugation or intermolecular  $\pi$ - $\pi$  interaction and provide potential for visible-light absorption. Therefore, pyrene-based metal-organic frameworks have attracted much attention as photocatalysts.<sup>29–32</sup>

Herein, a thermally stable two-dimensional cobalt-based metal-organic framework,  $\{[\text{Co}_2(\text{TBAPy})(\text{H}_2\text{O})_2] \cdot (\text{DMF})(\text{H}_2\text{O})_8\}_n$  (Co-TBAPy), was assembled successfully with the pyrene-based ligand H<sub>4</sub>-TBAPy (1,3,6,8-tetrakis(*p*-benzoic acid)pyrene) serving as a linker and cobalt as a node through a facile solvothermal method. Cooperating with [Ru(bpy)<sub>3</sub>]Cl<sub>2</sub>·6H<sub>2</sub>O as a photosensitizer and triethanolamine (TEOA) as a sacrificial agent, Co-TBAPy exhibits excellent photocatalytic performance towards CO<sub>2</sub> reduction under visible light, and can achieve a CO evolution rate of 1856.5  $\mu\text{mol g}^{-1} \text{h}^{-1}$ . Especially, the ratio of syngas (CO/H<sub>2</sub>) can be regulated in a wide range between 0.14 and 1.65 simply by adjusting the water content in the photocatalytic system, and a precise proportion of CO : H<sub>2</sub> = 1 : 2 and 1 : 3 favourable for fuel synthesis can be attained. Theoretical calculations were performed to clearly disclose the mechanisms.

## Results and discussion

Single-crystal X-ray diffraction verifies that Co-TBAPy crystallizes in a triclinic space group  $P\bar{1}$ , which is the same as that reported before (Table S1†).<sup>33</sup> Each asymmetric unit possesses a Co<sup>2+</sup> atom, a TBAPy<sup>4-</sup> ligand and a coordinated water molecule. In detail, Co-TBAPy is constructed from dinuclear Co<sub>2</sub>(CO<sub>2</sub>)<sub>4</sub> paddle-wheel secondary building units (SBUs) capped with two water molecules at the axial positions, which are further connected by four TBAPy<sup>4-</sup> ligands (Fig. 1a). It is due to the dinuclear paddle-wheel structure that gives rise to a two-

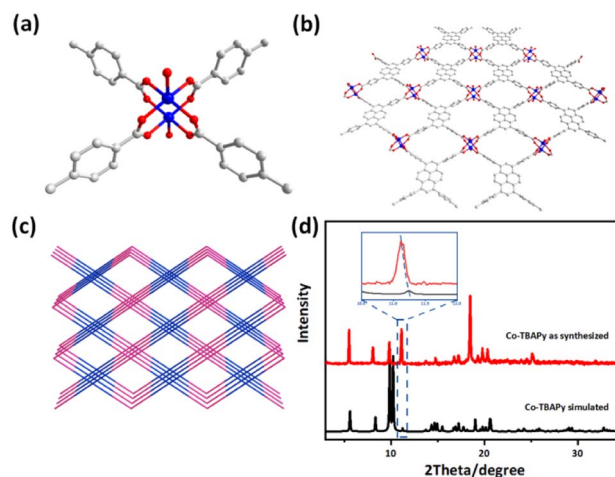


Fig. 1 Crystal structure of Co-TBAPy. (a) Coordination environment of Co<sup>2+</sup>, (b) 2D layer structure of Co-TBAPy along the *a*-axis, (c) simplified diagram for the packing of 2D layers with (4,4)-net topology, and (d) PXRD patterns of Co-TBAPy as-synthesized and simulated. Color representation: gray, C; red, O; blue, Co. H atoms are removed for clarity.

dimensional layered structure in Co-TBAPy equipped with two one-dimensional rhombus channels (size 6.34 × 7.18 Å and 7.21 × 9.08 Å, respectively) perpendicular to each layer (Fig. 1b). Confirmed by TOPOS software, Co-TBAPy retains a (4,4)-net topology, which can be simplified into an **sql** net (Fig. 1c). The crystal structure and refinement data of Co-TBAPy are supplied in Table S2.† As shown in the SEM images (Fig. S1†), Co-TBAPy presents a regular block shape with a flat surface, showing a thickness of ~7  $\mu\text{m}$  and a length of 20–50  $\mu\text{m}$ . To investigate the purity, the powder X-ray diffraction patterns (PXRD) of Co-TBAPy synthesized were obtained, which exhibited excellent consistency with the simulated one (Fig. 1d).

The powder of as-synthesized Co-TBAPy was immersed in various polar solvents, like acetone, methanol, ethanol, acetonitrile (MeCN), dimethylacetamide (DMA) and dichloromethane (DCM), in which Co-TBAPy can retain the pristine structure for 6 days at room temperature. Moreover, it can exist stably in water for 3 days. All of the PXRD diagrams without obvious changes have proved the solvent stability and universality of Co-TBAPy (Fig. S2†). Compared with the FT-IR spectrum of H<sub>4</sub>TBAPy, the disappearance of the hydroxyl vibration peak of –COOH in the range of 3400–3000  $\text{cm}^{-1}$  in the spectrum of Co-TBAPy illustrates the formation of Co–O bonds (Fig. S3†). Simultaneously, the peak at 1750–1620  $\text{cm}^{-1}$  originating from the vibration of the carbonyl group (–COOH) shifts to a lower wavenumber. Thermogravimetric (TG) analysis exhibits a weight loss of ~12.2% in the range of 98–180 °C, which is attributed to the loss of H<sub>2</sub>O. And the core frameworks of Co-TBAPy can remain intact even at 405 °C (Fig. S4†). Calculated by using PLATON software, the solvent accessible volume of Co-TBAPy is estimated to be 33.3% and the total potential solvent area volume is 376.6 Å<sup>3</sup>.

A type I isotherm was observed from the nitrogen adsorption/desorption curves at 77 K (Fig. 2a), indicating the presence

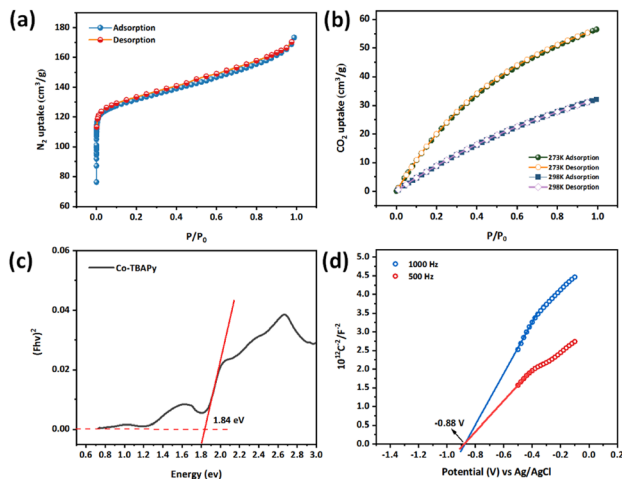


Fig. 2 (a)  $N_2$  adsorption–desorption isotherms at 77 K. (b)  $CO_2$  isotherms at 273 K and 298 K of Co-TBAPy. (c) Tauc plot of Co-TBAPy. (d) Mott–Schottky plot of Co-TBAPy at 500 Hz and 1000 Hz, respectively.

of micropores in Co-TBAPy. The Brunauer–Emmett–Teller (BET) surface area was calculated to be  $851 \text{ m}^2 \text{ g}^{-1}$  and the average pore width is evaluated to be  $\sim 0.67 \text{ nm}$ , demonstrating abundant potentially active sites for photocatalysis (Fig. S5<sup>†</sup>). Furthermore, Co-TBAPy displays a high affinity to  $CO_2$ , whose maximum adsorption capacity is measured to be  $56.5 \text{ cm}^3 \text{ g}^{-1}$  at 273 K (Fig. 2b). The adsorption enthalpy for carbon dioxide is calculated to be  $23.5\text{--}26.6 \text{ kJ mol}^{-1}$ , revealing that Co-TBAPy is a kind of potential material for photocatalytic reduction of  $CO_2$  (Fig. S6<sup>†</sup>).

The ultraviolet-visible absorption (UV-vis) spectrum shows that Co-TBAPy has excellent absorption capacity for visible light, in which the maximum adsorption value reaches 680 nm (Fig. S7<sup>†</sup>). As calculated by the Kubelka–Munk (K–M) method<sup>34</sup> (Fig. 2c), the band gap of Co-TBAPy is estimated to be 1.84 eV, unveiling its potential to be a kind of semiconducting photocatalyst. Mott–Schottky measurements on Co-TBAPy were conducted at 500 Hz and 1000 Hz, respectively (Fig. 2d). The positive slope of the curves elucidates that Co-TBAPy is a typical n-type semiconductor and its flat band position is determined to be  $\sim -0.88 \text{ V vs. Ag/AgCl}$  (*i.e.*,  $-0.68 \text{ V vs. NHE}$ ). Since it is generally accepted that the bottom of the conduction band (CB) of n-type semiconductors is more negative by about 0.1 V than the flat band position,<sup>35</sup> the CB of Co-TBAPy is forecasted to be  $-0.78 \text{ V vs. NHE}$ , which is more negative than the redox potential of  $E(CO_2/CO) = -0.53 \text{ V vs. NHE}$ .<sup>36</sup> In light of the band gap of 1.84 eV determined above, the value of the valence band (VB) is estimated to be  $1.06 \text{ V vs. NHE}$ .

Considering the prominent thermal and solvent stability, specific surface area, and the suitable band positions for  $CO_2$  redox potential, the  $CO_2$  photoreduction performance of Co-TBAPy under visible light was determined on a  $CO_2$ -saturated mixture of acetonitrile and water with  $[Ru(bpy)_3]Cl_2$  serving as a photosensitizer and TEOA acting as a sacrificial agent. CO was detected as the only carbonous product and  $H_2$  was discovered

as the byproduct using a gas chromatograph. As the illumination time increases, the evolution of CO increased rapidly, while the yield of  $H_2$  did not decrease significantly. As displayed in Fig. 3a and S8,<sup>†</sup> the amounts of CO and  $H_2$  reach  $27 \mu\text{mol}$  and  $156 \mu\text{mol}$  after 24 h illumination, in which the highest production yield of CO can reach  $990.8 \mu\text{mol g}^{-1} \text{ h}^{-1}$ . The turnover number (TON) is calculated to be 5.4 for CO and 31.2 for  $H_2$  according to the content of cobalt of Co-TBAPy used in photocatalysis.

To probe the key factors that influence the action of photocatalytic reduction of  $CO_2$ , a series of control experiments were conducted (Table S2<sup>†</sup>). In the absence of light,  $[Ru(bpy)_3]Cl_2 \cdot 6H_2O$  or TEOA, there are no gaseous products detected, unveiling that light, a photosensitizer and a sacrificial agent are essential for Co-TBAPy in the catalytic  $CO_2$  reduction process. Without Co-TBAPy, less CO and  $H_2$  are produced, which reveals that Co-TBAPy does play a catalytic role in the photoreduction process. While replacing  $CO_2$  with  $N_2$ , no CO was evolved. Isotopic  $^{13}CO_2$  labeling experiments verified  $CO_2$  as the only carbon source (Fig. 3b). Compared with the air sample, the peak at  $28 \text{ m/z}$  shown in Fig. 3b (left) originates from the  $N_2$  of air leaked in the injection needle. Furthermore, recycling experiments were conducted to examine the stability of Co-TBAPy. After three rounds of recycling tests, the photocatalytic activity is well maintained (Fig. 3c and S9<sup>†</sup>). Deduced from the PXRD pattern and FT-IR spectrum of Co-TBAPy after photocatalysis, Co-TBAPy retained integrated frameworks (Fig. S10 and S11<sup>†</sup>). Obviously, Co-TBAPy is manifested to be a stable heterogeneous catalyst for photocatalytic reduction of  $CO_2$ .

It is acknowledged that CO and  $H_2$  are the main components of syngas for methanol synthesis and the Fischer–Tropsch

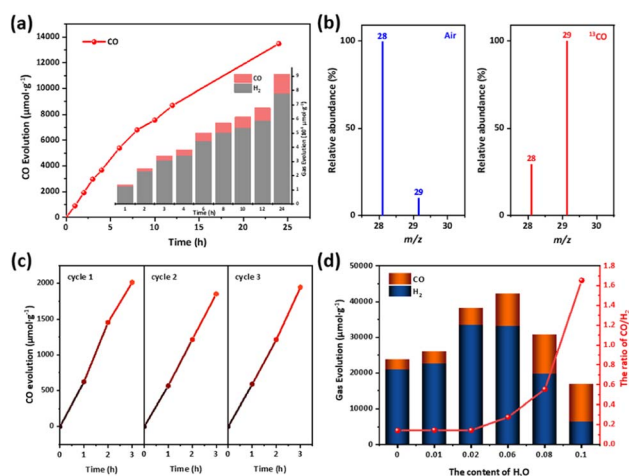


Fig. 3 (a) Time-dependent gas evolution of CO, and the inset image shows the  $H_2/CO$  ratio in  $CO_2$ -saturated MeCN solution (5 mL) containing Co-TBAPy (5  $\mu\text{mol}$ ),  $[Ru(bpy)_3]Cl_2$  (0.01 mmol), TEOA (1 mL) and  $H_2O$  (0.25 mL) at room temperature and irradiated with  $\lambda > 420 \text{ nm}$ . (b) GC-MS results of the isotopic experiment under a  $^{13}CO_2$  atmosphere (right) and for comparison, the air sample was detected. (c) The amounts of CO during three-run recycling experiments. (d) Plots of  $H_2/CO$  generation with the tuning of the ratio of  $H_2O$  under similar conditions for an 18 h reaction and the curve of the ratio of syngas ( $CO/H_2$ ) at different  $H_2O$  contents.



reaction.<sup>37</sup> Since the carbon product selectivity is wonderful without an excess carbonous product during the process of photocatalytic reduction of CO<sub>2</sub>, it is theoretically feasible to use the competitive reaction of hydrogen evolution to adjust the output of CO and H<sub>2</sub>, thereby realizing an adjustment of syngas in various ratios. Photocatalytic CO<sub>2</sub> reduction was performed under different contents of water added into MeCN solution. As shown in Fig. 3d, by using pure MeCN solvent without water, the evolution of CO (2924.2 μmol g<sup>-1</sup>) is less than that of hydrogen (20 893.7 μmol g<sup>-1</sup>). As the water content increases, the production of CO gradually increases, and the output of H<sub>2</sub> first increases accordingly but then decreases when the water content is higher than 8%. When the water content reaches 10%, the CO evolution can reach 37.13 μmol after 10 h irradiation, during which the highest CO production rate reaches 1856.5 μmol g<sup>-1</sup> h<sup>-1</sup> (Table S2,† entry 1). Evidently, by simply adjusting the water content of the system, we can achieve a wide range of controllable synthesis of the syngas ratio CO/H<sub>2</sub> from 0.14 to 1.65. As compared in Table S3,† in the current research on the photocatalytic reduction of CO<sub>2</sub> to produce controllable proportions of syngas, Co-TBAPy outperforms most MOF-based catalysts, homogeneous cobalt complexes and some inorganic semiconductors. It is worth mentioning that when using a H<sub>2</sub>O content of 6%, the evolution of CO and H<sub>2</sub> keeps a ratio nearly at 1:3, which can serve as raw materials for the synthesis of methane. Moreover, when the content of H<sub>2</sub>O goes up to 8%, the yield of CO and H<sub>2</sub> can achieve a ratio of 1:2, which is a profitable composition of syngas for methanol synthesis and industrial application in Fischer-Tropsch hydrocarbon formation.<sup>8,38,39</sup>

To obtain an in-depth understanding of the electron transfer process on photocatalytic CO<sub>2</sub> reduction, a series of characterization tests on Co-TBAPy were conducted. The photocurrent response curves of Co-TBAPy were investigated (Fig. S12†). A fast and regular photocurrent response was recorded for each light-on/off event under visible-light (λ > 420 nm) irradiation, indicating that the photogenerated electrons transferred quickly on the surface of Co-TBAPy without recombination. The steady state photoluminescence (PL) spectra and time-resolved transient PL decay spectra were investigated for the as-synthesized Co-TBAPy and ligand H<sub>4</sub>TBAPy. An obvious fluorescence quenching phenomenon and shorter lifetime appear on Co-TBAPy, demonstrating that photo-excited electron-hole pairs separated efficiently on the surfaces (Fig. 4a and S13†).

Comparing different types of photosensitizers, [Ru(bpy)<sub>3</sub>]Cl<sub>2</sub>·6H<sub>2</sub>O exhibited the best light absorption performance during the photocatalytic CO<sub>2</sub> reduction (Fig. S14†). The band energy-level accordance between Co-TBAPy and [Ru(bpy)<sub>3</sub>]Cl<sub>2</sub>·6H<sub>2</sub>O is a significant factor. The highest occupied molecular orbital (HOMO) and lowest unoccupied molecular orbital (LUMO) energy levels of [Ru(bpy)<sub>3</sub>]Cl<sub>2</sub>·6H<sub>2</sub>O are described to be 1.22 V and -1.27 V vs. NHE, respectively. As presented in Fig. 4b, the LUMO energy level is more negative than the CB position of Co-TBAPy, which is theoretically possible because photoexcited electrons can be transferred from the LUMO level of [Ru(bpy)<sub>3</sub>]Cl<sub>2</sub>·6H<sub>2</sub>O to the CB of Co-TBAPy to reduce the CO<sub>2</sub> molecules bound on cobalt sites. PL quenching measurements were conducted on the photocatalytic system in acetonitrile.

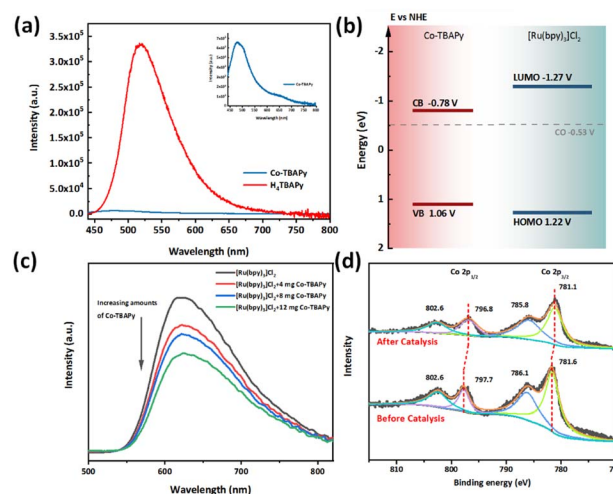
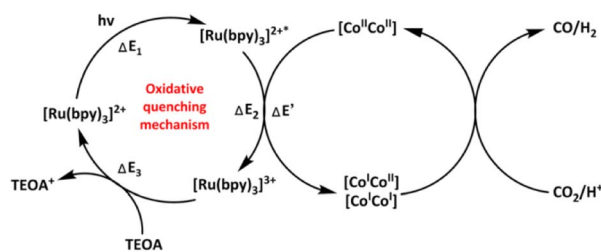


Fig. 4 (a) Photoluminescence (PL) spectra of as-synthesized Co-TBAPy and the ligand H<sub>4</sub>TBAPy (λ<sub>ex</sub> = 390 nm). (b) Schematic energy level diagram for Co-TBAPy and [Ru(bpy)<sub>3</sub>]Cl<sub>2</sub>. (c) Steady state fluorescence spectra of [Ru(bpy)<sub>3</sub>]Cl<sub>2</sub> upon the addition of increasing amounts of Co-TBAPy (λ<sub>ex</sub> = 395 nm). (d) The high resolution X-ray photoelectron spectroscopy (XPS) of the Co 2p orbit of Co-TBAPy before and after photocatalysis.

With the increasing amounts of Co-TBAPy, the PL intensity of excited [Ru(bpy)<sub>3</sub>]Cl<sub>2</sub>·6H<sub>2</sub>O gradually diminished, unveiling an oxidative quenching mechanism for the excited state [Ru(bpy)<sub>3</sub>]<sup>2+\*</sup> where the excited electrons were transferred to Co-TBAPy (Fig. 4c).<sup>40</sup> In contrast, an evident enhanced PL intensity has arisen when different amounts of TEOA were added into [Ru(bpy)<sub>3</sub>]Cl<sub>2</sub>·6H<sub>2</sub>O (Fig. S15†).

Moreover, high resolution X-ray photoelectron spectroscopy (XPS) was carried out to analyze the composition and chemical states of elements in Co-TBAPy (Fig. 4d and S16†). Before photocatalysis, the binding energies at 781.6 eV and 797.7 eV were ascribed to Co 2p<sub>3/2</sub> and Co 2p<sub>1/2</sub>, respectively, accompanied by two satellite peaks at 786.1 eV and 802.6 eV, attributed to the shakeup excitation of high-spin Co<sup>2+</sup> ions.<sup>41</sup> After photocatalysis, a slight shift to a lower Co binding energy was observed, disclosing that some of the cobalt atoms on the surface received electrons during photocatalysis, together with a coordination environment change of cobalt.<sup>42</sup> Analogously, the XPS spectrum of Co 3s displays a strong splitting attributed to the 3d<sup>7</sup> high-spin configuration of Co<sup>2+</sup> (S = 3/2) before photocatalysis, while after photocatalysis, only a single peak at 102.5 eV is observed (Fig. S17†).<sup>43</sup> These results further confirmed that Co sites served as an electron transfer intermediate station during the photocatalytic process, which can receive electrons from the photosensitizer and then transfer to the bound CO<sub>2</sub>.

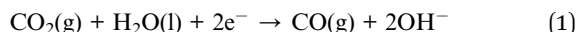
On the basis of the above photocatalytic results and physical characterization, a possible mechanism of photocatalytic reduction of CO<sub>2</sub> in the Co-TBAPy participated system is proposed (Scheme 1). Under visible-light irradiation, the light absorber [Ru(bpy)<sub>3</sub>]Cl<sub>2</sub>·6H<sub>2</sub>O is excited to generate photo-excited electron-hole pairs, in which photogenerated electrons migrate to the Co sites by oxidative quenching and excited state [Ru(bpy)<sub>3</sub>]<sup>2+\*</sup> is reduced by the electron donor TEOA. Then the CO<sub>2</sub> molecules



Scheme 1 Proposed catalytic mechanism for the photocatalytic reduction of CO<sub>2</sub> catalyzed by Co-TBAPy.

absorbed on Co-TBAPy accept electrons from cobalt sites to form CO, accompanied by hydrogen evolution. Among these processes, adjusting the water content in the photocatalytic system can provide alterable protons for the formation of CO. Meanwhile, H<sub>2</sub>O molecules can stabilize the CO<sub>2</sub> reaction intermediate through the hydrogen bonding effect. It might result in a more favorable CO<sub>2</sub>RR than the HER when a higher water content is involved, which effectively realizes the controlled synthesis of syngas in different proportions.

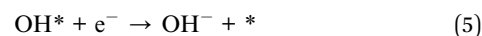
Density functional theory (DFT) calculations were carried out to reveal the effect of the water content on the performance of Co-TBAPy photocatalytic reduction of CO<sub>2</sub> to syngas with a wide range of adjustable ratios (Fig. S18<sup>†</sup> manifesting the calculated configurations).<sup>44–46</sup> The band gap of a photocatalyst is crucial to determine its catalytic performance; therefore, the band structure of Co-TBAPy is first calculated as shown in Fig. S19,<sup>†</sup> giving the band gap at 1.79 eV, in reasonable agreement with the experimental results. In addition, the density of states (DOS) of Co-TBAPy also unveils that the bottom of the conduction band is mainly contributed by the Co and C atoms while the top of the valence band is mainly contributed by the C atoms. Next, we considered the reaction mechanism of photocatalytic CO<sub>2</sub> reduction over Co-TBAPy.<sup>47,48</sup> As shown in Fig. 3d, the evolution of CO gradually increases as the H<sub>2</sub>O content increases to a maximum of 8% and then slightly drops at 10%. According to the literature, with the presence of water in the MeCN solvent, the CO formation reaction may proceed *via* a proton-coupled electron transfer between CO<sub>2</sub> and H<sub>2</sub>O (eqn (1)).<sup>49</sup>



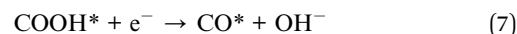
in which the presence of H<sub>2</sub>O as a proton source may facilitate the CO formation. Furthermore, in the cases of some cobalt complexes, H<sub>2</sub>O molecules stabilize the CO<sub>2</sub> molecules bound to the catalyst by forming hydrogen bonds, which also promotes the CO formation. Based on the above two facts, we propose that the interaction and charge transfer between CO<sub>2</sub> and H<sub>2</sub>O are crucial for the mechanism of the CO formation reaction catalyzed by Co-TBAPy. However, the origin of the dependence of CO evolution on the H<sub>2</sub>O content remains unclear. To unravel the reaction mechanism, we investigated both the H<sub>2</sub>O activation and hydrogen bond interaction which are proposed to be important for the HER and CO<sub>2</sub>RR.<sup>50,51</sup> We found that, for single molecule adsorption, the adsorption of H<sub>2</sub>O over a Co site is much stronger (adsorption energy

$E_{\text{ads}} = -1.23$  eV) than that of CO<sub>2</sub> ( $E_{\text{ads}} = -0.25$  eV), indicating a preference towards H<sub>2</sub> evolution rather than the CO<sub>2</sub>RR under a low H<sub>2</sub>O content (Fig. S20<sup>†</sup>).<sup>52</sup> With an extra electron addition to Co-TBAPy, CO<sub>2</sub> only physisorbs on Co with up to 4H<sub>2</sub>O molecules surrounded (Fig. 5a i–iii). Interestingly, CO<sub>2</sub> chemisorbs on Co with more than five H<sub>2</sub>O molecules presented (Fig. 5a iv and v). Upon chemisorption, CO<sub>2</sub> attaches to Co *via* a side-on configuration with one of its C=O double bonds.<sup>53,54</sup> Bader charge analysis shows that barely no electrons are accumulated on the CO<sub>2</sub> molecule upon physisorption ( $-0.03\text{e}^-$  for (CO<sub>2</sub> + 2H<sub>2</sub>O) and (CO<sub>2</sub> + 3H<sub>2</sub>O) systems and  $-0.04\text{e}^-$  for (CO<sub>2</sub> + 4H<sub>2</sub>O)), while considerable electrons transfer from the catalyst to CO<sub>2</sub> in chemisorbed (CO<sub>2</sub> + 5H<sub>2</sub>O) and (CO<sub>2</sub> + 6H<sub>2</sub>O) systems ( $-0.47\text{e}^-$  and  $-0.44\text{e}^-$ , respectively).

As a further stage in understanding the activity difference of Co-TBAPy in the HER and CO<sub>2</sub>RR and explaining the experimental observation, we investigated the reaction pathways for both the HER and the CO<sub>2</sub>RR involving different numbers of water molecules using the computational hydrogen electrode (CHE) method (Fig. 5b and c and S20).<sup>55,56</sup> According to a previous study, HER pathways can be summarized as the following four elementary steps under alkaline and neutral conditions:<sup>57</sup>



For the CO<sub>2</sub>RR under a low water content (corresponding to the scenarios in which less than five H<sub>2</sub>O molecules are involved), we proposed that H<sub>2</sub>O adsorption and dissociation first occur due to the preferred H<sub>2</sub>O adsorption on Co. The adsorption species OH\* and H\* can be obtained after H<sub>2</sub>O dissociation. Then OH\* accepts electrons and desorbs from the Co site, which facilitates an interaction between CO<sub>2</sub> and remaining H\* to form an intermediate COOH\*. It is followed by the dissociation of COOH\* into a CO\* intermediate and OH<sup>-</sup>. Finally, CO is obtained after desorption. All the processes are summarized as follows:



On the other hand, for the CO<sub>2</sub>RR under a higher water content (corresponds to the scenarios in which five and six H<sub>2</sub>O molecules are involved), CO<sub>2</sub> chemisorption is most likely achieved and its reduction to CO is possible as proposed below:<sup>58</sup>



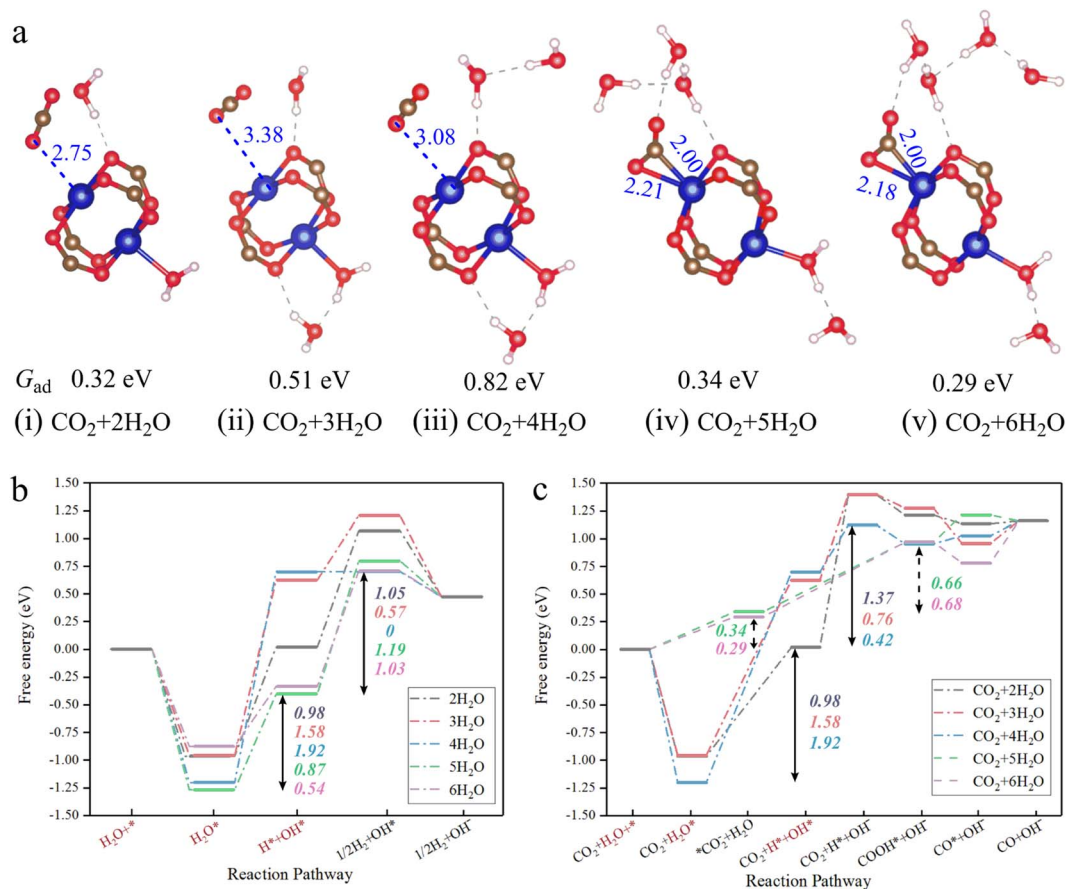
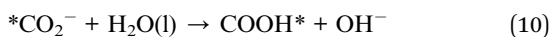


Fig. 5 (a) The configuration of CO<sub>2</sub> adsorption on Co-TBAPY and corresponding adsorption free energy at 298 K, which involves different numbers of H<sub>2</sub>O molecules: (i) two H<sub>2</sub>O, (ii) three H<sub>2</sub>O, (iii) four H<sub>2</sub>O, (iv) five H<sub>2</sub>O, and (v) six H<sub>2</sub>O. The brown dashed line labels the hydrogen bonding, while the blue dashed line represents the distance between atoms. (b and c) Calculated free energy diagrams for the photocatalytic HER (b), and CO<sub>2</sub>RR to CO (c) involving a multiple number of H<sub>2</sub>O molecules (pH = 8 and at 0 V vs. RHE). \* represents an active site.



We can find that under a low water content (corresponding to the scenarios with two to four H<sub>2</sub>O molecules), the reaction mechanisms of both the HER and the CO<sub>2</sub>RR go through *via* the process of H<sub>2</sub>O adsorption and dissociation. Considering the fact that the H<sub>2</sub>O dissociation (H<sub>2</sub>O\* → H\* + OH\*) is a common step for the HER and CO<sub>2</sub>RR, although it is also the determining step for systems with 3H<sub>2</sub>O or 4H<sub>2</sub>O, the competition of the HER and CO<sub>2</sub>RR is determined by the elementary steps with maximum reaction energy subsequent to (H<sub>2</sub>O\* → H\* + OH\*) for each reaction process, *i.e.* H\* → 1/2 H<sub>2</sub> (eqn (4)) for the HER and OH\* + e<sup>-</sup> → OH<sup>-</sup> + \* (eqn (5)) for the CO<sub>2</sub>RR, which is 1.05 eV vs. 1.37 eV for the 2H<sub>2</sub>O system, 0.57 eV vs. 0.76 eV for the 3H<sub>2</sub>O system, and 0 vs. 0.42 eV for the 4H<sub>2</sub>O system. Therefore, the HER is more preferred than the CO<sub>2</sub>RR due to the lower reaction free energy of H\* → 1/2 H<sub>2</sub> along the HER compared to that of OH\* + e<sup>-</sup> → OH<sup>-</sup> + \* along the CO<sub>2</sub>RR under a low water content.

Meanwhile under a higher water content (corresponding to the scenarios with five and six H<sub>2</sub>O molecules involved in the reaction), the HER is now determined by using H\* → 1/2 H<sub>2</sub> (eqn (4)). On the other hand, the CO<sub>2</sub>RR will not go through H<sub>2</sub>O dissociation but direct protonation to \*COOH due to the

presence of CO<sub>2</sub> chemisorption, and its determining step becomes \*CO<sub>2</sub><sup>-</sup> + H<sub>2</sub>O(l) → COOH\* + OH<sup>-</sup> (eqn (10)). In these cases, the competition of the HER and CO<sub>2</sub>RR is controlled by the reaction free energies of the corresponding determining steps (*i.e.* eqn (4) and (10), respectively). The calculated reaction free energies are 1.19 and 1.03 eV for H\* → 1/2 H<sub>2</sub> (eqn (4)) along the HER pathway in 5H<sub>2</sub>O and 6H<sub>2</sub>O systems, respectively, while the calculated reaction free energies are 0.66 and 0.68 eV for \*CO<sub>2</sub><sup>-</sup> + H<sub>2</sub>O(l) → COOH\* + OH<sup>-</sup> (eqn (10)) along the CO<sub>2</sub>RR pathway in 5H<sub>2</sub>O and 6H<sub>2</sub>O systems, respectively. Therefore, the CO<sub>2</sub>RR shows lower reaction free energy than the HER and thus the CO<sub>2</sub>RR suppresses the HER under a high water content. These computational results are consistent well with the experiments, showing promise to control the ratio of CO : H<sub>2</sub> in syngas photosynthesis from CO<sub>2</sub> reduction by using Co-based MOFs as a photocatalyst and water content as a modulator.

## Experimental section

### Chemicals and characterization

All reagents of analytical grade were acquired through commercial channels and used without further purification.



The PXRD spectra were recorded on a Rigaku SmartLab X-ray diffractometer using Cu-K $\alpha$  radiation ( $\lambda = 1.54056 \text{ \AA}$ ) at room temperature. The SC-XRD data were recorded at the SSRF (Shanghai Synchrotron Radiation Facility) 14B beamline. The X-ray photoelectron spectroscopy (XPS) data were collected on an ESCALab 250 using a monochromatic Al K $\alpha$  radiation source. The FT-IR spectra were collected on a Nicolet/Nexus-670 spectrometer using a KBr disk. The thermogravimetric (TG) analyses were performed on a NETZSCH TG209 system in nitrogen with a heating rate of  $5 \text{ }^\circ\text{C min}^{-1}$ . The Brunauer–Emmett–Teller (BET) specific surface area and pore volume were analysed by using a Quantachrome Autosorb-iQ2-MP gas adsorption analyzer. The gases ( $\text{N}_2$  and  $\text{CO}_2$ ) used in the gas adsorption measurements hold ultra-high purity. The morphology of the samples was determined by using an ultra-high resolution field emission scanning electron microscope (SEM, SU8010). The UV-vis absorption data were obtained on a SHIMADZU UV-3600 equipped with an integrating sphere using  $\text{BaSO}_4$  as a reference. Photoluminescence (PL) and time-resolved fluorescence decay spectroscopy were performed on an EDINBURGH FLS980 fluorescence spectrophotometer.

### Synthesis of Co-TBAPy $\{[\text{Co}_2(\text{TBAPy})(\text{H}_2\text{O})_2] \cdot (\text{DMF})(\text{H}_2\text{O})_8\}_n$

The crystals of Co-TBAPy were obtained by a facile solvothermal method between  $\text{H}_4\text{TBAPy}$  (1,3,6,8-tetrakis(*p*-benzoic acid)pyrene) (0.015 mmol) and  $\text{Co}(\text{NO}_3)_2 \cdot 6\text{H}_2\text{O}$  (0.1 mmol) in a mixed solution of DMF,  $\text{H}_2\text{O}$ , dioxane and concentrated hydrochloric acid (v/v/v/v, 2/1/1/0.01) at  $120 \text{ }^\circ\text{C}$  for 3 days. Green transparent flake crystals were collected and washed with DMF and acetone, respectively (yield at  $\sim 76.5\%$ , based on ligands). The Co-TBAPy synthesized was soaked in acetone for 3 days, during which the acetone was changed every 12 h. After that, Co-TBAPy was filtered and dried in an oven at  $100 \text{ }^\circ\text{C}$  for 12 h and activated Co-TBAPy was obtained. Elemental analysis: found for  $\text{C}_{47}\text{H}_{49}\text{O}_{19}\text{NCO}_2$ : C 53.49, H 4.14, N 0.95%; calcd: C 53.77, H 4.67, N 1.33%.

### Photocatalytic test

Photocatalytic carbon dioxide reduction tests were carried out in a 54 mL closed Pyrex reactor with a LED lamp (light intensity:  $100 \text{ mW cm}^{-2}$ , PCX50B Discover multi-channel photochemical reaction system, Beijing Perfectlight Technology Co., Ltd) serving as a visible light source. Typically, the catalyst Co-TBAPy (0.005 mmol, activated) and  $[\text{Ru}(\text{bpy})_3]\text{Cl}_2 \cdot 6\text{H}_2\text{O}$  (0.01 mmol) were dispersed in an acetonitrile aqueous solution of different ratios, in which TEOA (1 mL) acted as a sacrificial agent to suppress the oxidation half reaction. Then the reaction flask was evacuated and filled with  $\text{CO}_2$ , repeated three times before the irradiation. The gas products were detected by using a gas chromatograph (GC9790, Fuli Analytical Instrument Co., Ltd) with a thermal conductivity detector (TCD) for  $\text{H}_2$  detection and a flame ionization detector for CO detection.

### Photoelectron measurement

All of the photoelectric tests adopted a standard three-electrode system, consisting of a platinum plate electrode ( $1 \text{ cm} \times 1 \text{ cm}$ )

as the counter electrode, Ag/AgCl as the reference electrode and MOF catalyst coated fluorine doped tin oxide (FTO) glass as the working electrode with a working area of  $0.5 \times 0.5 \text{ cm}^2$ . In detail, 5 mg of Co-TBAPy samples and 20  $\mu\text{L}$  Nafion D-520 dispersion (5% w/w in water and 1-propanol) were added into 0.5 mL of ethanol and then ultrasonicated for 5 min to obtain a suspension. 0.2 mL of the suspension liquid was added dropwise onto the FTO glass and the coating area was restricted to  $0.25 \text{ cm}^2$  by using insulating tape. The well coated FTO glass was dried at  $85 \text{ }^\circ\text{C}$  for a day. The electrolyte was 0.5 M sodium sulfate aqueous solution. Both Mott–Schottky measurements and photocurrent response tests were performed on a CHI 660E electrochemical analyzer (CH Instruments, Chenhua Co., Shanghai, China). The Mott–Schottky measurements were performed at 500 Hz and 1000 Hz, respectively, with an amplitude at 0.01 V. During the photocurrent response tests, a Xe Lamp (300 W,  $\lambda > 420 \text{ nm}$ , CEL-HXF300, Beijing Aulight Co.) served as the visible light source. The on–off cycle of illumination was manually controlled by the operator at a time interval of 5 s.

### Computational details

All calculations were performed in a spin-polarized fashion and by using the VASP code based on plane-wave basis sets. The generalized gradient approximation (GGA) with the Perdew–Burke–Ernzerhof (PBE) functional was for the exchange–correlation functional. Projector augmented wave (PAW) potentials were used for electron–ion interactions with an energy cutoff of 500 eV. The energy and force convergence settings were  $10^{-5} \text{ eV}$  and  $0.02 \text{ eV } \text{\AA}^{-1}$ , respectively. Hubbard U correction was also introduced for the Co atom with  $U_{\text{eff}} = 3.3$ . The *k*-point mesh was set to be  $4 \times 2 \times 2$  for geometry optimization and  $8 \times 5 \times 3$  for electronic structure calculations. The cell parameter of Co-TBAPy after the optimization is  $6.72 \text{ \AA} \times 10.85 \text{ \AA} \times 16.06 \text{ \AA}$ ,  $\alpha = 90.00$ ,  $\beta = 90.00$ , and  $\gamma = 102.01$ , in agreement with the experimental results.

As it is known that  $\text{H}_2$  evolution and the  $\text{CO}_2\text{RR}$  go through a process containing proton–electron pair transfer, the computational hydrogen electrode (CHE) method thus was used to calculate the free energy of each intermediate state, of which the free energy of proton–electron pairs ( $\text{H}^+ + \text{e}^-$ ) equals  $\frac{1}{2}\text{H}_2(\text{g})$ . The Gibbs free energy change ( $\Delta G$ ) for each elemental step is calculated by

$$\Delta G = \Delta E + \Delta E_{\text{ZPE}} - T\Delta S + \Delta G_{\text{pH}}$$

where  $\Delta E$  is the electronic energy difference between free standing and adsorption states of reaction intermediates;  $\Delta E_{\text{ZPE}}$  and  $\Delta S$  are the changes of zero point energy and entropy, respectively, which are obtained based on vibrational calculations.  $T$  is the temperature and set to be 298 K in this work and pH is set to be 8 because acetonitrile is the solvent.  $\Delta G_{\text{pH}} = 2.303k_{\text{B}}T \times \text{pH}$ , where  $k_{\text{B}}$  is the Boltzmann constant. The free energy of CO was calculated from the known free energy change (0.21 eV) of the reaction  $\text{CO}_2(\text{g}) + 2\text{H}^+ + 2\text{e}^- = \text{CO}(\text{g}) + \text{H}_2\text{O}(\text{l})$  under the standard conditions. The  $\text{CO}_2\text{RR}$  involves two

electron transfers, while the HER involves one electron transfers, and after the correction of  $\Delta G_{\text{pH}}$ , the final  $\Delta G = 0.21 + 0.47 \times 2 = 1.15$  eV for the CO<sub>2</sub>RR and  $\Delta G = 0.47$  eV for the HER. The adsorption energy ( $E_{\text{ad}}$ ) is computed by using the formula:

$$E_{\text{ad}} = E_{\text{sub+A}} - E_{\text{sub}} - E_{\text{A}} \quad (11)$$

where  $E_{\text{sub+A}}$ ,  $E_{\text{sub}}$  and  $E_{\text{A}}$  represent the total energies of the substrate with adsorbed species and the pure substrate without the adsorbate and adsorbate, respectively. And  $G_{\text{ad}}$  is the corresponding adsorption free energy at 298 K.

## Conclusions

In summary, a 2D cobalt-based metal-organic framework consisting of dinuclear Co<sub>2</sub>(COO)<sub>4</sub> paddle-wheel SBUs and TBAPy<sup>4-</sup> ligands with extended  $\pi$ -systems was synthesized by a facile solvothermal method and used as a stable photocatalyst to photoreduce CO<sub>2</sub> to syngas under visible light. Notably, the ratio of syngas as-prepared (CO/H<sub>2</sub>) can be adjusted in a wide range between 0.14 and 1.65 simply by adjusting the water content in the photocatalytic system. The proportion of syngas with CO : H<sub>2</sub> = 1 : 2 and 1 : 3 was achieved respectively, which is desirable for the practical applications of methanol and methane synthesis. Photocatalytic experiments, characterization and DFT calculation elucidate the probable electron transfer processes, and the thermodynamic and kinetic feasibility of Co-TBAPy serving as a photocatalyst. This work might present a new low-cost metal-organic framework semiconductor for the artificial photosynthesis of syngas and a more accessible preparation route of syngas at various ratios.

## Conflicts of interest

There are no conflicts to declare.

## Acknowledgements

This work was supported by the NKRD Program of China (2021YFA1500401), the NSFC Projects (22171291, 21720102007, 21821003, and 21890380), the Local Innovative and Research Teams Project of Guangdong Pearl River Talents Program (2017BT01C161), and the FRF for the Central Universities. We thank Prof. Pengbo Lv of Xiangtan University for help in theoretical discussions.

## References

- S. C. Peter, *ACS Energy Lett.*, 2018, **3**, 1557–1561.
- R. P. Ye, J. Ding, W. Gong, M. D. Argyle, Q. Zhong, Y. Wang, C. K. Russell, Z. Xu, A. G. Russell, Q. Li, M. Fan and Y. G. Yao, *Nat. Commun.*, 2019, **10**, 5698.
- S. Bai, H. Qiu, M. Song, G. He, F. Wang, Y. Liu and L. Guo, *eScience*, 2022, **2**, 428–437.
- J. Li, Y. He, L. Tan, P. Zhang, X. Peng, A. Oruganti, G. Yang, H. Abe, Y. Wang and N. Tsubaki, *Nat. Catal.*, 2018, **1**, 787–793.
- V. N. Nguyen and L. Blum, *Chem. Ing. Tech.*, 2015, **87**, 354–375.
- J. S. Lee, D. I. Won, W. J. Jung, H. J. Son, C. Pac and S. O. Kang, *Angew. Chem., Int. Ed.*, 2017, **56**, 976–980.
- M. Sun, C. Wang, C. Y. Sun, M. Zhang, X. L. Wang and Z. M. Su, *J. Catal.*, 2020, **385**, 70–75.
- X. Wang, Z. L. Wang, Y. Bai, L. Tan, Y. Q. Xu, X. J. Hao, J. K. Wang, A. H. Mahadi, Y. F. Zhao, L. R. Zheng and Y. F. Song, *J. Energy Chem.*, 2020, **46**, 1–7.
- H. W. Zhang, J. T. Ming, J. W. Zhao, Q. Gu, C. Xu, Z. X. Ding, R. S. Yuan, Z. Z. Zhang, H. X. Lin, X. X. Wang and J. L. Long, *Angew. Chem., Int. Ed.*, 2019, **58**, 7718–7722.
- C. Qiu, X. Hao, L. Tan, X. Wang, W. Cao, J. Liu, Y. Zhao and Y. F. Song, *Chem. Commun.*, 2020, **56**, 5354–5357.
- A. Li, T. Wang, X. X. Chang, Z. J. Zhao, C. C. Li, Z. Q. Huang, P. P. Yang, G. Y. Zhou and J. L. Gong, *Chem. Sci.*, 2018, **9**, 5334–5340.
- H. Furukawa, K. E. Cordova, M. O’Keeffe and O. M. Yaghi, *Science*, 2013, **341**, 1230444.
- T. Ghanbari, F. Abnisa and W. M. A. Wan Daud, *Sci. Total Environ.*, 2020, **707**, 135090.
- M. Pan, W.-M. Liao, S.-Y. Yin, S.-S. Sun and C.-Y. Su, *Chem. Rev.*, 2018, **118**, 8889–8935.
- Y. Shi, A. F. Yang, C. S. Cao and B. Zhao, *Coord. Chem. Rev.*, 2019, **390**, 50–75.
- I. I. Alkhatib, C. Garlisi, M. Pagliaro, K. Al-Ali and G. Palmisano, *Catal. Today*, 2020, **340**, 209–224.
- X. Feng, Y. Pi, Y. Song, C. Brzezinski, Z. Xu, Z. Li and W. Lin, *J. Am. Chem. Soc.*, 2020, **142**, 690–695.
- Q.-L. Hong, H.-X. Zhang and J. Zhang, *J. Mater. Chem. A*, 2019, **7**, 17272–17276.
- M. Liu, Y.-F. Mu, S. Yao, S. Guo, X.-W. Guo, Z.-M. Zhang and T.-B. Lu, *Appl. Catal., B*, 2019, **245**, 496–501.
- S. Fu, S. Yao, S. Guo, G.-C. Guo, W. Yuan, T.-B. Lu and Z.-M. Zhang, *J. Am. Chem. Soc.*, 2021, **143**, 20792–20801.
- S. Guo, L.-H. Kong, P. Wang, S. Yao, T.-B. Lu and Z.-M. Zhang, *Angew. Chem., Int. Ed.*, 2022, **61**, e202206193.
- Y. Qin, Y. Wan, J. Guo and M. Zhao, *Chin. Chem. Lett.*, 2022, **33**, 693–702.
- J.-W. Wang, L.-Z. Qiao, H.-D. Nie, H.-H. Huang, Y. Li, S. Yao, M. Liu, Z.-M. Zhang, Z.-H. Kang and T.-B. Lu, *Nat. Commun.*, 2021, **12**, 813.
- T.-C. Zhuo, Y. Song, G.-L. Zhuang, L.-P. Chang, S. Yao, W. Zhang, Y. Wang, P. Wang, W. Lin, T.-B. Lu and Z.-M. Zhang, *J. Am. Chem. Soc.*, 2021, **143**, 6114–6122.
- X.-K. Wang, J. Liu, L. Zhang, L.-Z. Dong, S.-L. Li, Y.-H. Kan, D.-S. Li and Y.-Q. Lan, *ACS Catal.*, 2019, **9**, 1726–1732.
- Z. Wang, C.-Y. Zhu, H.-S. Zhao, S.-Y. Yin, S.-J. Wang, J.-H. Zhang, J.-J. Jiang, M. Pan and C.-Y. Su, *J. Mater. Chem. A*, 2019, **7**, 4751–4758.
- H. Yang, D. Yang and X. Wang, *Angew. Chem., Int. Ed.*, 2020, **59**, 15527–15531.
- J. Zhao, Q. Wang, C. Sun, T. Zheng, L. Yan, M. Li, K. Shao, X. Wang and Z. Su, *J. Mater. Chem. A*, 2017, **5**, 12498–12505.
- Y. Xiao, Y. Qi, X. Wang, X. Wang, F. Zhang and C. Li, *Adv. Mater.*, 2018, **30**, e1803401.



- 30 T. C. Wang, W. Bury, D. A. Gomez-Gualdron, N. A. Vermeulen, J. E. Mondloch, P. Deria, K. Zhang, P. Z. Moghadam, A. A. Sarjeant, R. Q. Snurr, J. F. Stoddart, J. T. Hupp and O. K. Farha, *J. Am. Chem. Soc.*, 2015, **137**, 3585–3591.
- 31 T. Islamoglu, S. Goswami, Z. Li, A. J. Howarth, O. K. Farha and J. T. Hupp, *Acc. Chem. Res.*, 2017, **50**, 805–813.
- 32 A. Gladysiak, T. N. Nguyen, R. Bounds, A. Zacharia, G. Itkos, J. A. Reimer and K. C. Stylianou, *Chem. Sci.*, 2019, **10**, 6140–6148.
- 33 Y.-D. Huang, J.-H. Qin, X.-G. Yang, H.-R. Wang, F.-F. Li and L.-F. Ma, *J. Solid State Chem.*, 2020, **285**, 121252.
- 34 N. Li, J. Liu, J. J. Liu, L. Z. Dong, Z. F. Xin, Y. L. Teng and Y. Q. Lan, *Angew. Chem., Int. Ed.*, 2019, **58**, 5226–5231.
- 35 J. He, J. Wang, Y. Chen, J. Zhang, D. Duan, Y. Wang and Z. Yan, *Chem. Commun.*, 2014, **50**, 7063–7066.
- 36 J. Schneider, H. Jia, J. T. Muckerman and E. Fujita, *Chem. Soc. Rev.*, 2012, **41**, 2036–2051.
- 37 H. Xu, S. You, Z. Lang, Y. Sun, C. Sun, J. Zhou, X. Wang, Z. Kang and Z. Su, *Chem.–Eur. J.*, 2020, **26**, 2735–2740.
- 38 J. R. Rostrup-Nielsen, *Catal. Today*, 2000, **63**, 159–164.
- 39 X. Gu, L. Qian and G. Zheng, *Mol. Catal.*, 2020, **492**, 110953.
- 40 A. N. Radhakrishnan, P. P. Rao, K. S. M. Linsa, M. Deepa and P. Koshy, *Dalton Trans.*, 2011, **40**, 3839–3848.
- 41 B. Zhou, X. Zhao, H. J. Liu, J. H. Qu and C. P. Huang, *Appl. Catal., B*, 2010, **99**, 214–221.
- 42 M.-J. Wei, J.-H. Zhang, W.-M. Liao, Z.-W. Wei, M. Pan and C.-Y. Su, *J. Photochem. Photobiol., A*, 2020, **387**, 112137.
- 43 L. Dahéron, R. Dedryvère, H. Martinez, M. Ménétrier, C. Denage, C. Delmas and D. Gonbeau, *Chem. Mater.*, 2008, **20**, 583–590.
- 44 G. Kresse and J. Hafner, *Phys. Rev. B*, 1993, **47**, 558–561.
- 45 K. B. John, P. Perdew and M. Ernzerhof, *Phys. Rev. Lett.*, 1996, **77**, 3865–3868.
- 46 P. E. Blochl, *Phys. Rev. B*, 1994, **50**, 17953–17979.
- 47 Y. Kuramochi, O. Ishitani and H. Ishida, *Coord. Chem. Rev.*, 2018, **373**, 333–356.
- 48 Y. Yamazaki, H. Takeda and O. Ishitani, *J. Photochem. Photobiol., C*, 2015, **25**, 106–137.
- 49 M. C. Figueiredo, I. Ledezma-Yanez and M. T. M. Koper, *ACS Catal.*, 2016, **6**, 2382–2392.
- 50 S. Chen, X. Li, C.-W. Kao, T. Luo, K. Chen, J. Fu, C. Ma, H. Li, M. Li, T.-S. Chan and M. Liu, *Angew. Chem., Int. Ed.*, 2022, **61**, e202206233.
- 51 J. S. Derrick, M. Loipersberger, S. K. Nistanaki, A. V. Rothweiler, M. Head-Gordon, E. M. Nichols and C. J. Chang, *J. Am. Chem. Soc.*, 2022, **144**, 11656–11663.
- 52 A. Behera, A. K. Kar and R. Srivastava, *Mater. Horiz.*, 2022, **9**, 607–639.
- 53 J.-C. Jiang, J.-C. Chen, M.-d. Zhao, Q. Yu, Y.-G. Wang and J. Li, *Nano Res.*, 2022, **15**, 7116–7123.
- 54 W. Gao, Z. Li, Q. Han, Y. Shen, C. Jiang, Y. Zhang, Y. Xiong, J. Ye, Z. Zou and Y. Zhou, *Chem. Commun.*, 2022, **58**, 9594–9613.
- 55 A. A. Peterson, F. Abild-Pedersen, F. Studt, J. Rossmeisl and J. K. Nørskov, *Energy Environ. Sci.*, 2010, **3**, 1311–1315.
- 56 Y. Lan, Y. Xie, J. Chen, Z. Hu and D. Cui, *Chem. Commun.*, 2019, **55**, 8068–8071.
- 57 X. Zheng, Y. Yao, W. Ye, P. Gao and Y. Liu, *Chem. Eng. J.*, 2021, **413**, 128027.
- 58 Y.-R. Wang, Q. Huang, C.-T. He, Y. Chen, J. Liu, F.-C. Shen and Y.-Q. Lan, *Nat. Commun.*, 2018, **9**, 4466.